Macromolecules

ARTICLE

pubs.acs.org/Macromolecules

Molecular Exchange in Ordered Diblock Copolymer Micelles

Soo-Hyung Choi,[†] Frank S. Bates,[*,†] and Timothy P. Lodge[*,†,‡]

[†]Department of Chemical Engineering and Materials Science and [‡]Department of Chemistry, University of Minnesota Minneapolis, Minnesota 55455, United States

Supporting Information

ABSTRACT: Molecular exchange kinetics of diblock copolymers forming spherical micelles packed on a body-centered cubic (bcc) lattice were investigated using time-resolved small-angle neutron scattering (TR-SANS). Ordered arrays of polystyrene spheres were prepared by mixing 15 vol % poly(styrene-*b*-ethylene-*alt*-propylene) (PS−PEP) in squalane, a highly selective solvent for the PEP block. Two pairs of diblock copolymers were examined, characterized by two different PS core block molecular weights ($\langle M_{PS} \rangle$ = 26500 and 42800). Each pair contained two nearly identical diblock copolymers, one with a deuterated PS block (dPS−PEP) and the other with a protonated PS block (hPS−PEP). Protonated and deuterated squalane were blended to achieve a contrast-matched condition with uniformly mixed dPS and hPS (50/50 by volume) core chains. Beginning with a statistically random array of pure dPS and hPS cores distributed on the bcc lattice, molecular exchange was monitored at multiple temperatures by TR-SANS. Exchange of deuterated and protonated chains results in a decay in SANS intensity, which yields a kinetic function revealing a broad spectrum of relaxation times. These results are qualitatively consistent with our previously reported findings for molecular exchange between PS−PEP micelles in a dilute (1 vol %) squalane solution. However, the measured characteristic time constant for the concentrated, ordered system is more than an order of magnitude slower than in the dilute, disordered dispersion.

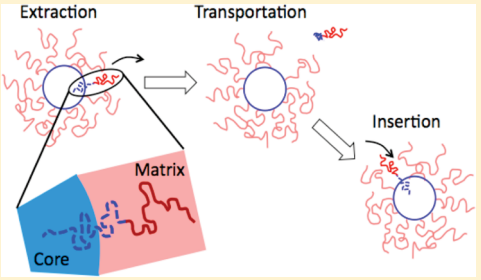

INTRODUCTION

Diblock copolymers can self-assemble into micelles or vesicles when dispersed in a medium that solvates one block selectively. Experimental emphasis has been focused on variations in micelle structure as a function of block copolymer composition, molecular weight, and concentration.[1] Less attention has been paid to the dynamics of chain exchange between block copolymer micelles. The strong thermodynamic incompatibility between the core blocks and the medium, coupled with the relative length of core blocks, leads to highly retarded exchange rates. Several techniques have been applied to investigate chain exchange kinetics for block copolymer micelles, including sedimentation,[2] temperature jump experiments,[3−6] nonradiative energy transfer and fluorescence quenching methods,[7−11] transmission electron microscopy,[12−14] and small-angle neutron scattering (SANS).[15−20] In spite of theoretical analysis[21−23] as well as extensive experimentation, the detailed mechanisms of chain exchange at dynamic equilibrium and during polymeric micelle assembly and disassembly have not been fully resolved. Recently, we characterized chain exchange for 1 vol % poly(styrene-*b*-ethylene-*alt*-propylene) (PS−PEP) dispersed in squalane by time-resolved small-angle neutron scattering (TR-SANS) and observed a quasi−logarithmic decay in relaxation time,[20] consistent with the work of Lund et al. on poly(ethylene-*alt*-propylene-*b*-ethylene oxide) (PEP−PEO) in aqueous solution.[17,18] On the basis of these experimental findings, we proposed that molecular exchange kinetics are governed by single chain exchange between micelles, which inherently involves unfavorable interactions between the core block segments and the medium. Consistent with the pioneering theory of Halperin and Alexander,[21] the proposed model predicts that the kinetics display a hypersensitivity to the degree of polymerization of the core block, thus polydispersity, which is corroborated by the experimental data.

As the concentration of spherical micelles formed by diblock copolymer increases, the micelles begin to overlap and eventually pack onto either face-centered cubic (fcc) or body-centered cubic (bcc) lattices, depending on the detailed form of the intermicellar potential.[24−28] Here, we consider whether the concentration of micelles affects single chain exchange kinetics. Provided that the micelle structure is independent of micelle concentration, the exchange rate might be expected to be nearly independent of micelle concentration if the extraction of a single molecule is rate-limiting. In this study, we address molecular exchange kinetics in diblock copolymer micelles using 15 vol % polymer solutions of 50% hPS−PEP and 50% dPS−PEP in an isotopic squalane mixture. Under these conditions, a well-defined bcc phase exists. We have chosen a combination of experimental parameters (i.e., isotopic labeling) such that all interparticle SANS scattering initially vanishes, resulting in an intensity that is proportional to the square of the concentration of hPS (or dPS) chains in the micelle cores. This condition mirrors the circumstances created for the previous study of dilute PS−PEP spherical micelles in squalane, where interparticle interference

Received: December 7, 2010
Revised: March 15, 2011
Published: April 07, 2011

Table 1. Diblock Copolymer Characteristics

polymer	N_{PS}[a]	N_{PEP}[b]	M_w/M_n
hPS−PEP-1	250	970	1.04
dPS−PEP-1	260	985	1.10
hPS−PEP-2	400	880	1.05
dPS−PEP-2	423	926	1.10

[a] Number of PS repeat units. [b] Number of PEP repeat units.

was negligible due to the low concentration.[20] The current results are discussed in comparison with the behavior of dilute solutions, and thereby provide further insight into the mechanisms that control molecular exchange in block copolymer dispersions.

EXPERIMENTAL SECTION

Materials. Two pairs of poly(styrene-*b*-ethylene-*alt*-propylene) (PS−PEP) diblock copolymers were synthesized using anionic polymerization of poly(styrene-*b*-isoprene) (PS−PI), followed by selective saturation of the PI block with deuterium, following established techniques.[29] Each matched pair includes perdeuterated styrene (Polymer Source, Inc.) (dPS−PEP) and protonated styrene (hPS−PEP). Isoprene and both perdeuterated and protonated styrene were purified with *n*-butyl lithium and dibutyl magnesium for 4 h, respectively. Isoprene monomer was initiated by *sec*-butyl lithium and polymerized in cyclohexane for 8 h at 40 °C. An aliquot (∼3 mL of solution) was then extracted from the reactor and terminated in degassed methanol. The PI block was characterized by size exclusion chromatography using a refractive index detector. Subsequently, styrene monomer was added and polymerized for at least 8 h at 40 °C. Degassed methanol was injected into the reactor to terminate the polymerization. The PS−PI diblock copolymer was then recovered by precipitation in methanol.

The PS−PI diblock copolymers were selectively saturated using a homogeneous Ni/Al catalyst.[30] A catalyst solution was prepared by adding 6 mL of triethylaluminum (Sigma-Aldrich) to 20 mL of 0.1 M nickel 2-ethylhexanoate (Sigma-Aldrich) stirred in cyclohexane under argon. A polymer solution in cyclohexane and the catalyst solution were injected into a stainless steel reactor at room temperature. The reactor was then charged with deuterium (400 psi, Cambridge Isotope Laboratories) and heated to 77 °C for at least 24 h. The PS−PEP diblock copolymer was recovered by stirring with 8 wt % citric acid in water until the catalyst color disappeared, followed by filtration with activated alumina and precipitation in methanol.

The polymers were characterized by size exclusion chromatography (SEC) and ^{1}H nuclear magnetic resonance spectroscopy (^{1}H NMR, Varian Inova 300). SEC was used to give the molecular weight of the PI aliquot by universal calibration based on ten PS standards, and the overall polydispersity (M_w/M_n) of all diblock copolymers. Molecular weights of PS−PI diblocks were computed by the molecular weights of the initiated PI block determined by SEC, and the masses of isoprene and styrene subsequently added to the reactor. The actual block copolymer compositions were verified by ^{1}H NMR spectroscopy indicating that complete addition of monomers was achieved. The extent of PI saturation was measured by ^{1}H NMR spectroscopy (>99%). Molecular characteristics of the four polymers are given in Table 1. The number of deuteriums per repeat unit in the PEP block was estimated to be 2.3 using ^{1}H NMR, which indicates a slight isotopic exchange during saturation.[31] An isotopic solvent mixture of 42 vol % protonated squalane (h-squalane, Sigma-Aldrich) and 58 vol % perdeuterated squalane (d-squalane, C/D/N Isotopes) was used to contrast match a 50/50 mixture of dPS and hPS in the micelle cores, as will be discussed in more detail later.

Sample Preparation. For this experiment, 15 vol % polymer solutions with either hPS−PEP or dPS−PEP were prepared by dissolving the polymers in the isotopic squalane mixture with dichloromethane as a cosolvent, followed by removal of the dichloromethane at room temperature. The polymer solutions were then annealed for 5 min at 150 and 170 °C for PS−PEP-1 and PS−PEP-2, respectively. The annealing temperatures were selected to be well above (∼50 °C) the temperature where molecular exchange was observed in dilute solution, yet still below the order−disorder transition.[20,29] The polymer solutions were then cooled down to room temperature where the PS cores become glassy. Subsequently, hPS−PEP and dPS−PEP polymer solutions were blended (50/50 by volume) using a cup-rotor mixer (CSI, MiniMax with a rotor diameter of 13 mm) at room temperature to produce "postmixed" specimens. The ability of the mixer to generate completely random arrangements of hPS−PEP and dPS−PEP micelles on a bcc lattice has been recently documented.[32] "Premixed" specimens were prepared by codissolving hPS−PEP and dPS−PEP (50/50 by volume) in squalane with dichloromethane as a cosolvent, followed by removal of the latter.

Time-Resolved Small-Angle Neutron Scattering (TR-SANS). TR-SANS experiments were performed on the NG7 30 m instrument at the Center for Neutron Research located at the National Institute of Standards and Technology, Gaithersburg, MD.[33] Scattering data were acquired with a neutron wavelength λ of 7 Å and a wavelength spread $\Delta\lambda/\lambda$ of 0.11. A sample to detector distance of 11 m was used to provide a q range of 0.005 Å^{-1} < q < 0.03 Å^{-1}, where q is the scattering wave vector defined as $q = 4\pi\lambda^{-1}\sin(\theta/2)$. A temperature-controlled electric heating block was used to maintain the sample temperature to within ±1 °C. The 15 vol % polymer solutions (hPS−PEP, dPS−PEP, postmixed, and premixed specimens) were loaded in quartz cells with ca. 1−1.5 mm thickness and exposed for 5−10 min at room temperature. Then, postmixed specimens were heated to a target temperature, and monitored by SANS every 5 min. Two-dimensional scattering data were corrected for detector sensitivity, sample transmission, empty cell scattering, and sample thickness and then azimuthally averaged and reduced to absolute intensity by the direct beam flux method. Data reduction was performed using the Igor package provided by NIST.[34]

Table 2 lists the calculated neutron scattering length density ρ of each material. The ρ_{sol} for the isotopic solvent mixture was estimated by $\rho_{sol} = \phi_{h\text{-squalane}}\rho_{h\text{-squalane}} + (1 - \phi_{h\text{-squalane}})\rho_{d\text{-squalane}}$, where $\phi_{h\text{-squalane}}$ is the volume fraction of h-squalane in the solvent mixture. $\phi_{h\text{-squalane}} = 0.42$ was used to match the scattering length density of a completely mixed 50/50 hPS/dPS micelle core (=3.93 × 10^{10} cm^{-2}) in this study.

Small-Angle X-ray Scattering (SAXS). SAXS experiments were conducted with the equipment maintained by the DuPont−Northwestern−Dow Collaborative Access Team at Argonne National Laboratory. Radiation of 17 keV, corresponding to a wavelength λ = 0.729 Å, and a sample-to-detector distance of 6.6 m were employed. Temperature was controlled by an electric heater under a slightly positive pressure of helium. The specimens, loaded in aluminum DSC pans, were annealed at the target temperature for at least 4 min, followed by X-ray exposure for 0.5−1 s. Two-dimensional SAXS images, collected using a MAR-CCD detector, were azimuthally averaged to one-dimensional plots of intensity versus q.

BACKGROUND

SANS. The scattering cross section $d\Sigma(q)/d\Omega$ of N spherical particles each composed of z scattering centers in solution is given by[35]

$$\frac{d\Sigma(q)}{d\Omega} = (\Delta\rho)^2\frac{v^2}{V}\{Nz^2P(q) + N^2z^2Q(q)\} \quad (1)$$

in which $P(q)$ and $Q(q)$ are the intraparticle and interparticle contributions, V and v are the system volume and the scattering center

Table 2. Scattering Length Densities

material	formula	molecular weight of repeat unit (g/mol)	density[a] (g/cm^3)	v^b (10^{-22} cm^3)	b^c (10^{-12} cm)	ρ (=b/v) (10^{10} cm^{-2})
d-squalane	$C_{30}D_{62}$	484	0.929	8.65	61.30	7.08
dPS	C_8D_8	112	1.128	1.65	10.66	6.46
hPS	C_8H_8	104	1.047	1.65	2.33	1.41
PEP	$C_5D_{2.3}H_{7.7}$	72.3	0.884	1.36	1.98	1.46
h-squalane	$C_{30}H_{62}$	422	0.810	8.65	−3.24	−0.374

[a] Density of deuterated material was calculated with the assumption that the volume per repeat unit is identical to that of protonated material. [b] Volume per repeat unit. [c] Coherent scattering length.

volume, respectively, and $\Delta\rho$ is the excess scattering length density of the scattering center against the background.

For a mixture of N_D deuterated and N_H protonated spheres, the scattering cross section can be expressed as

$$\frac{d\Sigma(q)}{d\Omega} = (\Delta\rho_D)^2\frac{v^2}{V}S_{DD}(q) + (\Delta\rho_H)^2\frac{v^2}{V}S_{HH}(q) + 2\Delta\rho_D\Delta\rho_H\frac{v^2}{V}S_{DH}(q) \quad (2)$$

where $S_{ij}(q)$ are partial structure factors defined by

$$S_{HH}(q) = N_H z^2 P(q) + N_H{}^2 z^2 Q_{HH}(q) \quad (3)$$

$$S_{DD}(q) = N_D z^2 P(q) + N_D{}^2 z^2 Q_{DD}(q) \quad (4)$$

$$S_{DH}(q) = N_H N_D z^2 Q_{DH}(q) \quad (5)$$

There is no intraparticle contribution for $S_{DH}(q)$ because two scattering centers cannot belong to the same sphere. If the H-spheres and D-spheres are perfectly randomly distributed on an ordered (e.g., bcc) lattice and any deuterium isotopic effects are negligible, it is reasonable to assume that $Q_{HH}(q) = Q_{DD}(q) = Q_{DH}(q) = Q(q)$. If the spheres are not randomly distributed on the lattice sites, then this assumption fails.

When the system includes an equal amount of H-spheres and D-spheres ($N_H = N_D = N/2$), eq 2 can be reduced to

$$\frac{d\Sigma(q)}{d\Omega} = \{(\Delta\rho_H)^2 + (\Delta\rho_D)^2\}\frac{v^2z^2N}{2V}P(q) + (\Delta\rho_H + \Delta\rho_D)^2\frac{v^2z^2N^2}{4V}Q(q) \quad (6)$$

where $P(q)$ and $Q(q)$ are separated. Equation 6 can be reorganized using $\Delta\rho_H = \rho_H - \rho_{sol}$ and $\Delta\rho_D = \rho_D - \rho_{sol}$ as

$$\frac{d\Sigma}{d\Omega}(q) = (\rho_D - \rho_H)^2\frac{v^2z^2N}{4V}P(q) + \left(\frac{\rho_H + \rho_D}{2} - \rho_{Sol}\right)^2\left\{\frac{v^2z^2N}{V}P(q) + \frac{v^2z^2N^2}{V}Q(q)\right\} \quad (7)$$

In eq 7, the first term is still the intraparticle scattering contribution with a different coefficient, which corresponds to the fluctuation between deuterated and protonated spheres. The second term, however, corresponds to the scattering obtained with fictitious spheres having an averaged scattering length density of deuterated and protonated spheres, i.e., $(\rho_H + \rho_D)/2$.[35,36]

When ρ_{sol} is designed to equal $(\rho_H + \rho_D)/2$ by blending protonated and deuterated solvent, the second term in eq 7 becomes zero. Here, the completely random distribution of H-spheres and D-spheres should be achieved. Under this condition, the intraparticle contribution (i.e., the spherical form factor) can be observed without interference from the interparticle contribution (i.e., Bragg scattering). Equation 7 is still satisfied, with appropriate modification of the coefficients, for arbitrary, nonspherical geometry (i.e., polymer chains) or for a ratio of H-spheres and D-spheres other than 1:1. This contrast matching technique, also known as the zero average contrast condition, has been used with SANS to measure single chain conformation in ordered block copolymer melts[37−40] and homopolymer melts and solutions.[35,41−45]

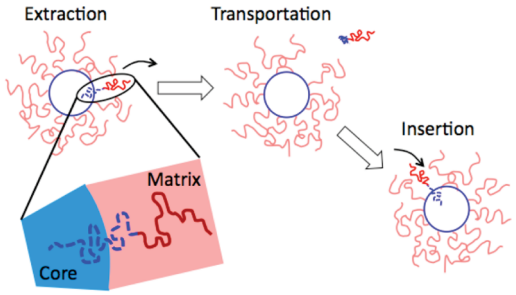

Figure 1. Schematic drawing for the single molecule exchange between micelles involving three steps: extraction of a core block, transportation of block copolymer through a solvent medium, and insertion into another micelle. Extraction of the core block carries the unfavorable interaction between the core block segments and solvent, and thus is rate-limiting.

Molecular Exchange Kinetics. Two primary mechanisms of exchange kinetics in diblock copolymer micelles have been proposed: (i) single chain insertion and expulsion, and (ii) micelle fusion and fission.[9,21,22,46] When the distribution of micelle size is narrow and close to equilibrium and corona brushes are relatively long (so-called star-like micelles), the micelle fusion/fission mechanism is known to be energetically unfavorable due to the repulsive interaction of micelle coronas.[18,21,22,46] Under this condition, the exchange kinetics of dilute PEP−PEO micelles in aqueous solution[18] and dilute PS−PEP micelles in squalane are independent of concentration (Supporting Information, Figure S1), which confirms suppression of the micelle fusion/fission mechanism. Therefore, the exchange kinetics are dominated by single chain insertion/expulsion, where a single macromolecule is extracted from a micelle, transported through a solvent medium, and inserted into another micelle as shown in Figure 1. Since polymer diffusion in low molecular weight solvents is much greater than in a polymer matrix,[47] the transport step is much faster than both the extraction and insertion. Furthermore, the core block must overcome unfavorable segment−solvent interactions during extraction; therefore, we assume that the extraction of the core block is rate-limiting.[19]

In our model, Rouse dynamics were used to estimate the longest relaxation time of the core block because weakly entangled polymers were employed in the study. The thermodynamic barrier due to the unfavorable interactions is assumed to be proportional to the product χN_{core} in which χ is the Flory−Huggins interaction parameter and N_{core} is the degree of polymerization of the core block.[48−51] Consequently, the time-correlation function for the chain extraction was expressed as

$$K(t, N_{core}) = \exp\left[-t\frac{6\pi^2 kT}{{N_{core}}^2 b^2 \zeta}\exp(-\alpha\chi N_{core})\right] \quad (8)$$

where k, T, b, ζ, and α are the Boltzmann constant, temperature, statistical segment length, monomeric friction factor, and an unknown prefactor of order unity, respectively. Accounting for the distribution in N_{core} using the Schulz−Zimm distribution $P(N_{core})$, the final expression of the relaxation function is

$$R(t) = \int_0^\infty P(N_{core})K(t, N_{core})\, dN_{core} \quad (9)$$

The double exponential dependence of N_{core} on $R(t)$ results in chain exchange kinetics that are hypersensitive to the core degree of polymerization, and therefore to polydispersity.[20]

Here, it is worthwhile to compare our model with that employed by Lund et al.[17,18] (based on the one originally developed by Halperin and Alexander[21]), which couples a Poisson distribution in core block lengths, or a Gaussian distribution of activation energies, with the extraction of core blocks. They assumed the single chain insertion/expulsion mechanism is dominant over the micelle fusion/fission mechanism, consistent with our model. This concept, which combined with a finite polydispersity, produced relatively poor agreement with their experimental data. As an alternative explanation, the necessity to rearrange core blocks prior to ejection was suggested to be responsible for the logarithmic decay of the relaxation time. This model is functionally similar to ours, however a key difference in our work is the investigation of diblock copolymers with different values of N_{core}, which directly exposes the hypersensitivity of $R(t)$ to this parameter after accounting for the effects of temperature. Subsequently, their model was modified to include a prefactor in a thermodynamic penalty (corresponding to α in our model) to intensify the N_{core} dependence on exchange kinetics.[52] The modified model, coupled with Poisson distribution in core block lengths, showed good agreement with their experimental data, qualitatively consistent with our conclusion. In their model, the thermodynamic penalty for the extraction of a core block was assumed to be proportional to ${N_{core}}^{2/3}$, rather than N_{core}, because core blocks were assumed to exist in a completely dry, collapsed state after ejection from the micelles; this restricts solvent-(core polymer) segment contact to the surface. However, a collapsed state formed by a single homopolymer chain in a poor solvent can contain a substantial amount of the solvent, suggesting that all or most monomers in the collapsed state can contact solvent molecules.[53,54] In addition, for block copolymer melt dynamics a dependence on N_{core} has been established.[50,51] Therefore, we have not assumed a completely collapsed core block (i.e., dense ball) in modeling $R(t)$, and hence, the thermodynamic penalty of core block extraction is proportional to N_{core}, rather than ${N_{core}}^{2/3}$.

RESULTS AND ANALYSIS

SAXS. The SAXS patterns in Figure 2 were obtained from 15 vol % polymer solutions of hPS−PEP, dPS−PEP, premixed, and postmixed for PS−PEP-1 and PS−PEP-2 both at room temperature, where there is no chain exchange between micelles (i.e., $T < T_{g,PS}$), and the higher temperature (i.e., 120 °C for PS−PEP-1 and 150 °C for PS−PEP-2), where SANS measurements were performed. All 16 diblock copolymer solutions form well-defined spherical micelles in squalane, which are packed onto a bcc lattice as evidenced by the sequence of peak ratios q/q^* (q^* is the primary peak) of $1{:}\sqrt{2}{:}\sqrt{3}{:}\sqrt{4}{:}\sqrt{5}{:}\sqrt{6}{:}\sqrt{7}$ (for the postmixed specimen of PS−PEP-1; up to $\sqrt{5}$ can be identified for the other specimens). Previous work showed that the micelle structure formed by 10 wt % solutions of the same block copolymers is nearly independent of temperature below the order−disorder transition that occurs above 200 °C.[29] Therefore, all the block copolymer micelles (15 vol %) packed onto bcc lattices at the temperatures of the TR-SANS measurements, as shown in Figure 2, parts b and d. The mismatch in peak positions between hPS−PEP and dPS−PEP (9% and 17% in nearest neighbor radius $R_{nn} = \sqrt{6}\pi/(2q^*) = \sqrt{3}a_{bcc}/4$, where a_{bcc} is the bcc lattice parameter, for PS−PEP-1 and PS−PEP-2, respectively) is attributed to the slight difference in block molecular weight. R_{nn} for postmixed and premixed specimens are the average of hPS−PEP and dPS−PEP, as expected.

Intraparticle scattering becomes dominant at higher q over interparticle scattering (i.e., Bragg scattering), as can be seen in Figures 2 for $q > 0.03$ Å^{-1}. We attempted to describe the former with the form factor $P_s(q)$ of uniform spheres of radius R_c,

$$P_s(q) = \left[\frac{3(\sin(qR_c) - qR_c\cos(qR_c))}{(qR_c)^3}\right]^2 \quad (10)$$

In order to account for the effect of variation in sphere size, a Gaussian distribution was incorporated while fitting the scattering data. Two fitting parameters (R_c and standard deviation σ_R) were adjusted using the Igor package provided by NIST.[34] The adjusted theoretical curves show good agreement with the observed scattering data for PS−PEP-2 at room temperature and the resulting parameters are provided in Table 3. We did not perform the fitting process for PS−PEP-1, since the scattering curves do not show distinct minima or maxima at higher q, leading to less confidence and precision in determining parameters.

The core radius R_c can be also estimated by the known structural symmetry and diblock copolymer composition. The number density of micelles n/V can be estimated as $2/(a_{bcc})^3$. The averaged aggregation number of the diblock copolymer in the micelles N_{agg} can be computed from n/V, the polymer volume fraction in solution (= 15 vol %), and the volume of the single chain v_{chain}, assuming no free chains. Consequently, the core radius of the micelle R_c can be computed as $R_c = (3v_{chain}N_{agg}/4\pi)^{1/3}$ with the assumption of no solvent penetration into the core at room temperature. The structural properties of the micelles thus calculated from the SAXS patterns are summarized in Table 3.

As can be seen in Table 4, both fitted and calculated R_c are approximately 20−30% bigger than R_c in 1 vol % dilute solution. Spherical micelles prefer to avoid significant corona overlap at higher micelle concentration, particularly when ordered on a lattice, leading to solutions with lower number densities of micelles, higher aggregation numbers, and hence larger spherical cores.[28]

SANS. Figure 3 displays the SANS data obtained from 15 vol % polymer solutions of hPS−PEP, dPS−PEP, premixed, and postmixed at 30 °C. Figure 3a shows the results for the PS−PEP-1 pair and Figure 3b shows the results for the PS−PEP-2 pair. For the hPS−PEP and dPS−PEP specimens, the SANS patterns reveal the

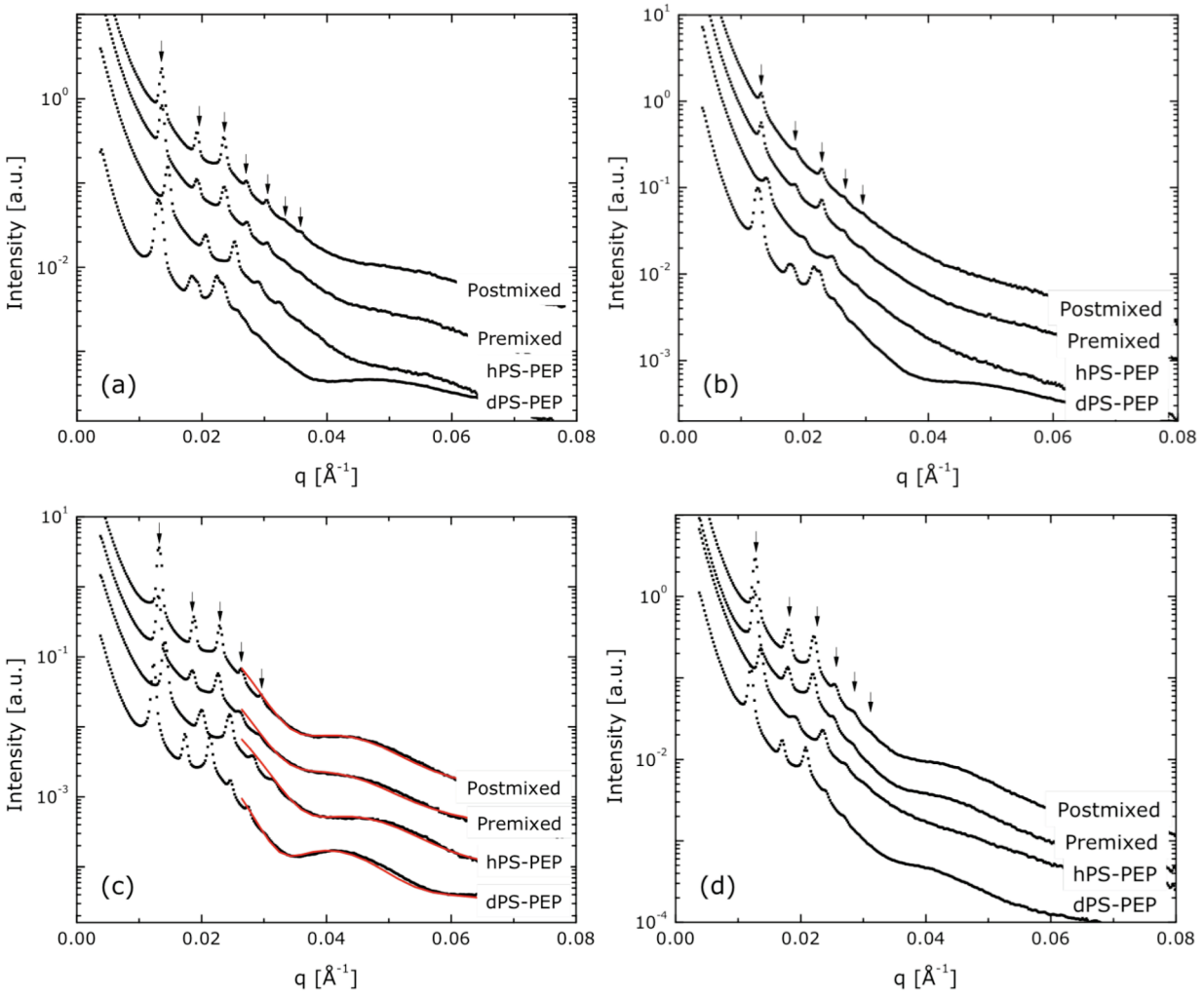

Figure 2. SAXS patterns obtained from 15 vol % polymer solutions in squalane: PS−PEP-1 (a) at room temperature and (b) at 120 °C, and PS−PEP-2 (c) at room temperature and (d) at 150 °C. Each plot includes data for dPS−PEP, hPS−PEP, premixed, postmixed as shown in the legend. The representative data for both polymers are indexed to bcc morphologies. Solid curves in (c) are the fits to a form factor of polydisperse PS spheres in the squalane matrix. Data are vertically shifted for convenience.

Table 3. Micelle Characteristics

		calculated properties from bcc lattice					fitting results[b]	
		q^* [Å^{-1}]	R_{nn} [Å]	a_{bcc} [Å]	n/V^a [10^{15} cm^{-3}]	R_c [Å]	R_c [Å]	σ_R [Å]
PS−PEP-1	dPS−PEP	0.0131	295	681	6.3	112	-	-
	hPS−PEP	0.0143	269	621	8.3	101	-	-
	premixed	0.0136	282	652	7.2	107	-	-
	postmixed	0.0136	282	652	7.2	107	-	-
PS−PEP-2	dPS−PEP	0.0122	315	728	5.2	136	130	17
	hPS−PEP	0.0143	269	621	8.3	116	114	18
	premixed	0.0132	291	672	6.6	126	121	21
	postmixed	0.0132	291	672	6.6	126	121	19

[a] ν_{chain} for premixed and postmixed solutions was calculated by averaging the values of dPS−PEP and hPS−PEP. [b] Fit to the form factor.

bcc structure identified by the relative peak positions q/q^* of $1{:}\sqrt{2}{:}\sqrt{3}$. The value of q^* for each pair between SAXS and SANS are identical, as indicated by arrows denoting the observed q^* in SAXS. However, SANS curves obtained from premixed and postmixed specimens show little or no evidence of bcc structure peaks. For premixed specimens this is due to negligible scattering contrast between the micelle cores and the medium, resulting in a masking out of the core contribution to the SANS intensity. Because of the bcc order and the noncontrast matched micelle coronas, small peaks are evident and correspond with q^* from SAXS (0.0136 and 0.0132 Å^{-1}

Table 4. Comparison of Micelle Characteristics between Dilute and Concentrated Solutions

	dilute micelle (1 wt %)[a]				ordered micelle (15 vol %)[b]			
	N_{agg}	R_h[c] [Å]	R_c [Å]	$\langle L\rangle = 2(R_h - R_c)$ [Å]	N_{agg}	R_{nn} [Å]	R_c [Å]	$\langle L\rangle = 2(R_{nn} - R_c)$ [Å]
PS−PEP-1	68	372	87	570	122	282	107	350
PS−PEP-2	84	392	110	564	124	292	126	332

[a] The values are taken from ref 29. [b] The values are averaged based in Table 3. [c] Hydrodynamic radius.

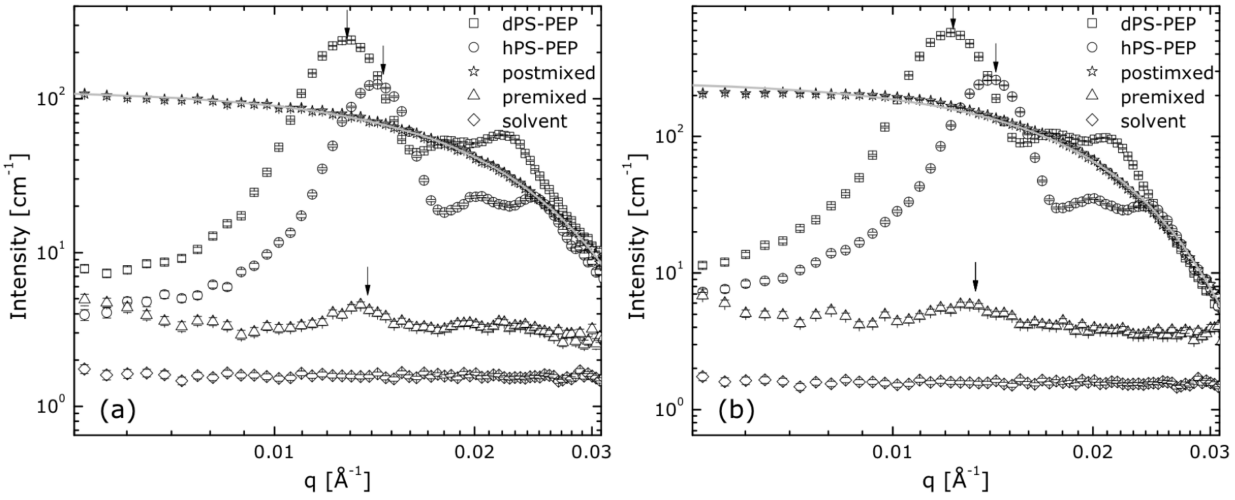

Figure 3. SANS patterns obtained from 15 vol % of (a) PS−PEP-1 and (b) PS−PEP-2 in squalane at 30 °C: dPS−PEP (square), hPS−PEP (circle), postmixed (star), premixed (triangle), and solvent (diamond) as shown in legend. Solid curves are best fit to eq 11. Arrows indicate the position of q^* observed in SAXS.

for PS−PEP-1 and PS−PEP-2, respectively), as indicated by arrows in Figure 3. Although fluctuations between deuterated and protonated PS chains in the cores are present, scattering from single PS core chains is also not detectable due to the overall low volume fraction of PS chains (ca. 4−5 vol %).

For the postmixed sample, the interparticle contribution (i.e., Bragg scattering) in SANS does not play a role under the experimental zero average contrast condition, as explained previously. This phenomenon can also be explained in analogous terms to crystal structures as observed in atomic binary solid solutions (i.e., $AuCu_3$).[55,56] When H-spheres and D-spheres are perfectly randomly distributed on bcc lattice sites, the probability of finding either an H-sphere or a D-sphere is 0.5. Therefore, it is reasonable to assume that fictitious spheres having a scattering length density of $\Delta\rho_{avg} = (\Delta\rho_H + \Delta\rho_D)/2$ occupy the sites. Under this experimental condition, $\Delta\rho_{avg}$ becomes zero and the crystal symmetry is invisible against the matrix. Consequently, interparticle scattering does not contribute to the SANS intensity. As a result the coherent scattering cross section for the postmixed specimens with the assumption of hard sphere of radius R_c and negligible corona scattering can be expressed as

$$\frac{d\Sigma(q)}{d\Omega} = \left(\frac{4\pi}{3}{R_c}^3\right)\phi_s(\rho_{core}(t) - \rho_{sol})^2 P_s(q) \qquad (11)$$

where ϕ_s is the volume fraction of spheres, $\rho_{core}(t)$ is time-dependent scattering length density of the micelle cores, and $P_s(q)$ is the spherical form factor as defined in eq 10.

The solid lines in Figure 3 are the best fits to eq 11 for postmixed samples by adjusting R_c and ϕ_s. The resulting R_c are 110 and 125 Å for PS−PEP-1 and PS−PEP-2, respectively, which are consistent with the fitted and calculated R_c by SAXS for postmixed specimens as indicated in Table 3. The fitted ϕ_s are 3.2 vol % and 5.0 vol % for PS−PEP-1 and PS−PEP-2, respectively. Considering the diblock copolymer composition, the PS volume fractions in the solution can be computed as 3.7 vol % and 5.5 vol % for PS−PEP-1 and PS−PEP-2, respectively, which shows reasonable agreement with the fitted values.

TR-SANS. Postmixed specimens containing 50% hPS−PEP and 50% dPS−PEP were heated to a target temperature and monitored by SANS every 5 min. Since the neutron scattering intensity is proportional to the square of the contrast against background, the intensity decreases as copolymers are exchanged between micelles. Figure 4 illustrates representative scattering curves obtained from postmixed specimens during time evolution at 119.5 and 156.5 °C for PS−PEP-1 and PS−PEP-2, respectively. The intensity decreases rapidly during the early stage, followed by a significant reduction in the rate of relaxation. In order to achieve annealing times longer than 3−4 h, specimens were maintained at the target temperature outside the SANS beamline and reinserted periodically. More than 13 h are required to achieve statistically distributed hPS and dPS in the cores. Note that any contribution from corona scattering is included in the premixed sample scattering, and is clearly negligible.

Since $(\rho_{core}(t) - \rho_{sol})$ in eq 11 is proportional to the volume fraction of hPS chains (or dPS chains) in the core, the scattering intensity is directly related to the extent of exchange. Therefore, the instantaneous state of exchange can be expressed by the normalized relaxation function $R(t)$ as

$$R(t) = \left(\frac{I(t) - I(\infty)}{I(0) - I(\infty)}\right)^{0.5} \qquad (12)$$

dx.doi.org/10.1021/ma102788v |Macromolecules 2011, 44, 3594–3604

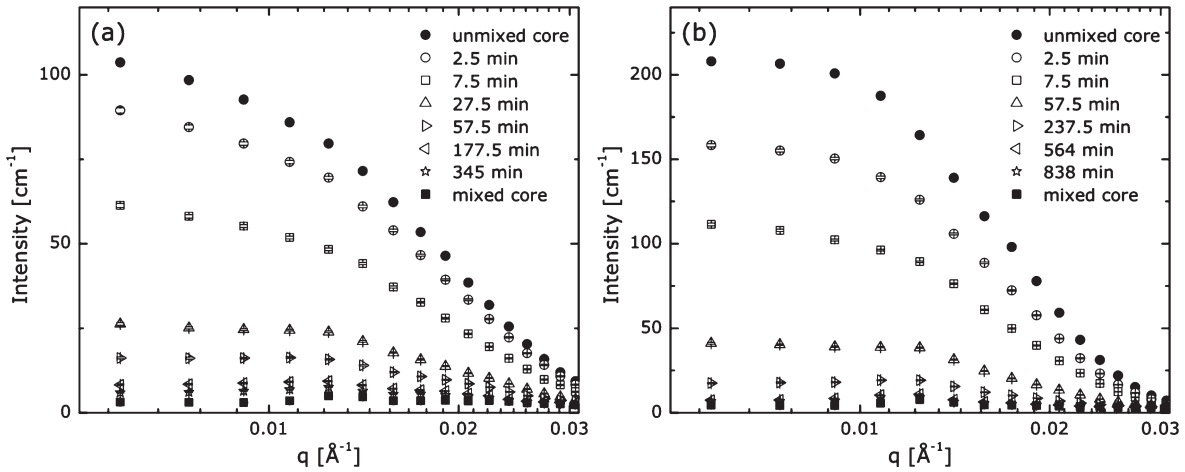

Figure 4. Time evolution of SANS patterns collected from a 15 vol % (a) dPS−PEP-1/hPS−PEP-1 50/50 mixture at 119.5 °C and (b) dPS−PEP-2/hPS−PEP-2 50/50 mixture at 156.5 °C. Initial measurements were obtained at 30 °C (filled circles), followed by the acquisition of SANS data every 5 min (shown in legend) at the target temperature. The statistically mixed core data were obtained from premixed specimens at the target temperature.

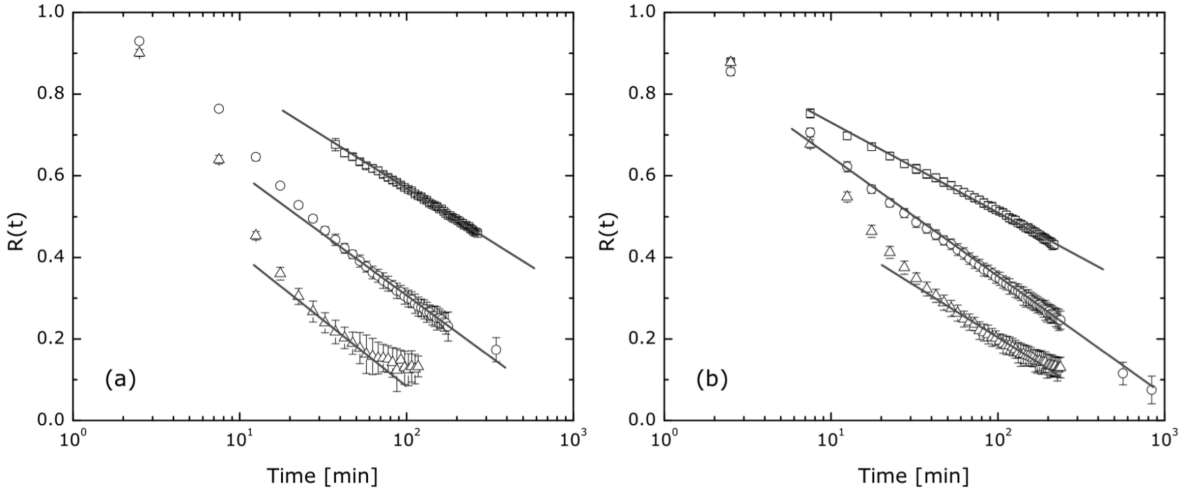

Figure 5. Relaxation function of (a) dPS−PEP-1/hPS−PEP-1 at 110 °C (squares), 119.5 °C (circles), and 130.3 °C (triangles) and (b) dPS−PEP-2/hPS−PEP-2 at 144.5 °C (squares), 156.5 °C (circles), and 164.5 °C (triangles). The straight lines are guides to the eye indicating logarithmic time dependence of relaxation decay.

where $I(0)$ and $I(\infty)$ is the neutron scattering intensity of the initial state, obtained from the postmixed specimen at 30 °C, and of the final state, obtained from the premixed specimen at the target temperature, respectively.[17,18] Figure 5 presents $R(t)$ plotted on a logarithmic time scale for PS−PEP-1 at 110, 119.5, and 130.3 °C, and for PS−PEP-2 at 144.5, 156.5, and 164.5 °C. The logarithmic form of $R(t)$ is consistent with our previous observations for the same copolymers in dilute solution[19] as well as the results of Lund et al. on PEP−PEO in aqueous solution.[17,18,52] This implies that the logarithmic decay is a result of single chain exchange that is hypersensitive to the core block length and therefore polydispersity, in a similar manner to the dilute solution.[20] The data at early times deviate from this function, in part because the temperature takes some time to stabilize, and in part because each point involves scattering integrated for 5 min.

It is worthwhile to compare $R(t)$ between the bcc-ordered state and the dilute solution to assess the expectation that the exchange rate is nearly independent of micelle concentration, based on the assumption that the extraction of the core block is rate-limiting. The average distance $\langle L \rangle$ an extracted chain must travel before encountering another micelle can be estimated based on the experimentally determined structural information. For the more concentrated (15 vol %) ordered mixtures, $\langle L \rangle$ = 350 and 332 Å for postmixed PS−PEP-1 and PS−PEP-2, respectively, where $\langle L \rangle = 2(R_{nn} - R_c)$. For the low concentration (1 wt %) disordered dispersions $\langle L \rangle = 2(R_h - R_c)$, where R_h is the hydrodynamic radius, resulting in distances of 570 and 564 Å for postmixed PS−PEP-1 and PS−PEP-2, respectively.[29] This assessment anticipates modestly shorter relaxation times for the ordered systems if the transport step is rate limiting.

The time−temperature superposition principle was applied in order to account for the effect of temperature. The TR-SANS data presented in Figure 6 were shifted to individual master curves at a reference temperature T_{ref} where the scattering intensities were monitored for both concentrations, i.e., T_{ref} = 110 °C for PS−PEP-1 and T_{ref} = 145 °C for PS−PEP-2, based on the shift factor $a_T = \tau(T)/\tau_{ref}(T_{ref})$ shown in the inset. Solid lines

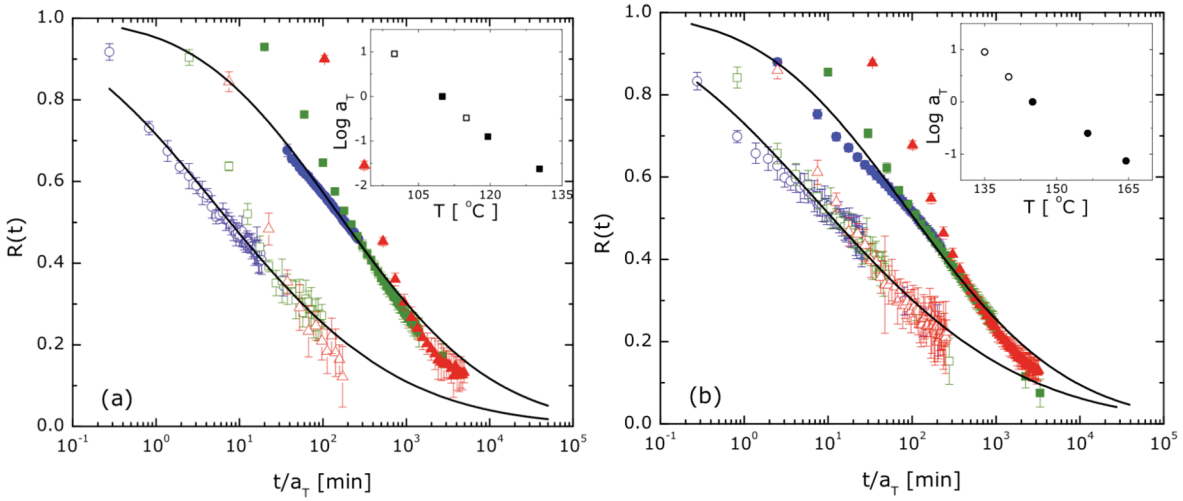

Figure 6. Comparison of time−temperature superposed $R(t)$ between dilute solution (open, regenerated from ref 19) and the bcc-ordered state (filled) for (a) PS−PEP-1 at T_{ref} = 110 °C [originally measured at 110 °C (filled circles), 119.5 °C (filled squares) and 130.3 °C (filled triangles)] and (b) PS−PEP-2 at T_{ref} = 145 °C [originally measured at 144.5 °C (filled squares), 156.5 °C (filled circles), and 164.5 °C (filled triangles)]. Solid curves are best fit to eq 9. The shift factors a_T are shown in the inset.

Table 5. Fitting Results for Relaxation Kinetics

		$\langle N_n \rangle$ (input)	N_w/N_n	$\alpha\chi$
PS−PEP-1[a]	dilute solution	255	1.07	0.045
	BCC-ordered state	255	1.03	0.057
PS−PEP-2[b]	dilute solution	412	1.05	0.036
	BCC-ordered state	412	1.03	0.041

[a] T_{ref} = 110 °C, $\zeta = 1.18 \times 10^{-7}$ N s m^{-1}. [b] T_{ref} = 145 °C, $\zeta = 2.41 \times 10^{-9}$ N s m^{-1}

are best fits to eq 9 by adjusting the thermodynamic penalty-related parameter $\alpha\chi$ and the polydispersity of the core block length. The monomeric friction factor ζ was estimated using reported rheology data for PS by shifting T_g to 70 °C to account for plasticization of PS due to solvent penetration into the core.[57] The statistical segment length was taken as 0.67 nm for PS.[58] The fitting results are summarized in Table 5. As illustrated in Figure 6, exchange kinetics of the bcc-ordered state are more than an order of magnitude slower than in dilute solution for both PS−PEP-1 and PS−PEP-2. This discrepancy is unanticipated, and is discussed in the following section.

DISCUSSION

We observed good agreement between the measured $R(t)$ for the bcc-ordered solutions and the relaxation function estimated by our model, with reasonable values of the fitting parameters, consistent with the behavior of the dilute solutions. $R(t)$ for the bcc-ordered solutions, however, is over an order of magnitude slower than for the corresponding dilute solutions, which is unexpected based on the assumption that the extraction of the core blocks is rate-limiting. We will investigate the sensitivity of the adjustable parameters in the model, followed by postulated reasons for these differences.

Sensitivity of Fitting Parameters. In this model, the chain exchange kinetics is determined by three factors: distribution of core block lengths, interactions between core block segments and solvent, and core block mobility. Core block polydispersity influences the breadth of the spectrum of relaxation times, and is associated with a specific slope to the logarithmic decay at intermediate time periods. As the polydispersity increases at fixed N_{core}, the distribution of exchange times changes significantly due to the double exponential dependence of $R(t)$ with respect to N_{core} [see Figure 4 in ref 20]. Therefore, we expect the slope of $R(t)$ to be independent of concentration for a given material. Within the uncertainties associated with the molecular characterization of the PS−PEP compounds and our determination of the time−temperature superposed relaxation times, we believe the slopes shown in Figure 6 are reasonably consistent with this expectation, i.e., the variation in the fitted polydispersities (Table 5) are within the collective uncertainty. However, the roughly 10-fold reduction in the rate of exchange dynamics for the bcc versus disordered mixtures is statistically relevant and far exceeds any recognized experimental error.

According to eqs 8 and 9, the unfavorable interactions between the core blocks and the matrix, expressed through χ, strongly influence the relaxation function $R(t)$ through the term $\alpha\chi$. Hence a 10% increase in $\alpha\chi$ induces approximately a 200% increase in the relaxation time (Supporting Information, Figure S2). Therefore, the slower dynamics documented for the bcc system leads to an increase in the apparent value of $\alpha\chi$ as shown in Table 5.

In the simplest description, χ accounts for the strength of the local interactions between polymer segments and solvent molecules independent of polymer chain length and concentration.[59,60] However, χ values between nonpolar solvents and nonpolar polymers are typically higher than 0.3, while for miscible polymer blends $\chi \approx O(10^{-2})$. Milner et al. suggested that this behavior is due mainly to entropic contributions to χ, which can be associated with the translational degrees of freedom required for the segments to explore free volume.[61] They noted that the thermal expansion coefficients for solvents (12×10^{-4} K^{-1}) are typically a factor of 1.7 greater than those for polymers (7×10^{-4} K^{-1}) and this difference suggests that solvent molecules can move more aggressively around the available free volume. On the basis of this observation Milner deduced that the entropic contribution to χ decreases as the length of solvent molecules increases. Since the thermal expansion coefficient of squalane (8.15×10^{-4} K^{-1}),[62] is close to that of linear polymer melts, it is a reasonable assumption that this solvent behaves more

like polymers than small molecules. Lund et al. reported that the calculated χ parameter between PS and *n*-alkanes decreases as the chain length increases for hydrocarbon solvents up to $n = 16$ based on Hildebrand's solubility parameters,[63] consistent with this argument. For these reasons, and because the segmental structure of squalane is identical to that of PEP, we assume that $\chi_{S\text{-squalene}}$ is identical to $\chi_{S\text{-EP}}$.

Sakurai et al. obtained the temperature dependence of $\chi_{S\text{-EP}}$ using solutions of PS−PEP ($M_n = 7.4 \times 10^4$ g/mol and $f_{PS} = 0.128$, where f_{PS} is the volume fraction of the PS block) in dioctyl phthalate (DOP) by interpreting SAXS patterns with the random phase approximation.[64] They estimated $\chi_{S\text{-EP}} = 0.07$ with a weak temperature dependence between 100 and 200 °C. Lai et al. measured the order−disorder temperature (T_{ODT}) for three PS−PEP block copolymers (2.0×10^4 g/mol $< M_w < 2.3 \times 10^4$ g/mol and $0.29 < f_{PS} < 0.35$), and reported a significantly larger and strongly temperature dependent segment−segment interaction parameter, $\chi_{S\text{-EP}} = 0.14$ at 100 °C and 0.09 at 200 °C.[65] This level of inconsistency in $\chi(T)$ based on estimates that rely on different experimental methods,[66] in this case the structure factor from SAXS versus T_{ODT}, directly influences our determination of the parameter α.

The prefactor α may be related to the shape of the potential at the interface between the core and the medium.[48] In the strong segregation regime polymer blocks tend to be completely segregated, producing a step-function-like composition profile at the interface. At weaker segregation strengths this profile broadens due to interfacial mixing, resulting in additional contacts between core block segments and the medium (i.e., solvent molecules or corona block segments). Hence, the thermodynamic penalty associated with extracting a core block into the matrix is reduced to a fraction of χN_{core},[67,68] which is manifested as a smaller value of α in the analysis of the block copolymer exchange dynamics. Provided $\chi_{S\text{-EP}}$ is approximately 0.1 at the experimental temperatures, the value of α ranges from 0.45 (PS−PEP-1) and 0.36 (PS−PEP-2) for the dilute solutions to 0.57 (PS−PEP-1) and 0.41 (PS−PEP-2) for the bcc-ordered mixtures, all consistent with theoretical expectations, i.e., lower than 1 and higher for the concentrated solutions.

Diffusion of diblock copolymers in bcc-ordered melt microstructures has been investigated using forced Rayleigh scattering (FRS),[51] forward recoil spectrometry (FRES),[50,69] and secondary mass ion spectrometry.[70] All results have shown that diffusion is strongly influenced by the enthalpic factor χN_{core}, resulting in $D = D_0 \exp[-\alpha \chi N_{core}]$ where D_0 is the diffusion coefficient in the absence of any interactions. Yokoyama and Kramer measured the self-diffusion of sphere forming asymmetric poly(styrene-*b*-2-vinylpyridine) using FRES and reported $\alpha = 1.2$.[50] Subsequent simulation results showed that α should be between 0 and 1.[68] Cavicchi and Lodge also reported α between 0.27 and 1.34 based on FRS experiments with four asymmetric poly(ethylene-*alt*-propylene-*b*-dimethylsiloxane) diblock copolymers.[51] While the variation in prior experimentally determined α values has not been resolved, they bracket the currently reported ones.

On the basis of Rouse dynamics, the longest relaxation time is inversely proportional to the core block mobility, which depends linearly on the monomeric friction factor ζ. At equilibrium, the micelle cores are slightly swollen and plasticized by solvent leading to a small reduction in the glass transition temperature and a modest increase in chain mobility, therefore a small reduction in ζ. Determining these variations in the PS−PEP/squalane mixtures is difficult due to the limited amount of PS present (<5% by volume of the total solvated specimens). However, independent differential scanning calorimetry experiments with PS−PI in squalane have revealed that $T_{g,PS}$ is nearly independent of concentration at lower polymer fraction (i.e., < 40 wt %),[71] which suggests that the difference in the solvent fraction in the presently reported micelle cores should be slight. Accordingly, we have applied the same value of ζ to both concentrations studied. However, it should be noted that the bcc micelle cores are larger than those in dilute solution, and thus $T_{g,PS}$ might be closer to the bulk value. Further experiments would be necessary to determine if this effect indeed plays a role.

Postulated Reasons for Slower Dynamics. We have documented that $R(t)$ is nearly independent of concentration between 0.5 vol % and 2 vol % of PS−PEP in squalane (Supporting Information, Figure S1), consistent with conclusions drawn by Lund et al.[18] Yet increasing the concentration to 15 vol %, and ordering on a cubic lattice, leads to a reduction by more than an order of magnitude in the rate of molecular exchange. The micelle structure and its surroundings may influence the overall exchange kinetics when contributions from these factors become significant relative to the core block dynamics as modeled by eqs 8 and 9. Here we consider two limiting scenarios: continuous changes coupled to the concentration of solvent, and discontinuous effects linked to micelle ordering.

Solvent plasticized core blocks experience a higher mobility and a reduced thermodynamic penalty for chain extraction relative to the undiluted melt state. Thus, increasing the block copolymer concentration, which lowers the tendency for solvent to penetrate the core, will slow molecular exchange. However, we suspect that such changes in core solvation are minimal, based on the glass transition results noted above, and we therefore doubt that this effect can fully explain the dramatic change in the recorded dynamics.

Ordering is accompanied by subtle but potentially significant modifications to the configuration of the core and corona blocks. Most obvious is the 20−30% increase in the core radii for the bcc arrangement relative to the 1% disordered solutions as described in Table 4. Since the core blocks are at most weakly entangled we do not anticipate this modest degree of stretching (the 1 wt % solutions core blocks are essentially relaxed, i.e., $R_c \sim N_{core}^{0.5}$)[29] to significantly affect the assumed Rouse dynamics or the thermodynamic penalty for chain extraction. The average configurational state of the corona chains also will be influenced to some extent by polymer concentration.

Increasing the block copolymer concentration brings corona chains from neighboring micelles into closer proximity, leading to overlap of the solvated PEP blocks. Such crowding ultimately induces ordering, where the bcc lattice offers the smallest variation in intermicellar spacings, relative to close-packed and other lower symmetry arrangements. Importantly, a crowded polymer environment will provide a further barrier to chain expulsion, beyond that embodied in χ, just as a single polymer would be more soluble in a dilute solution than a semidilute or concentrated one. This hypothesis does not distinguish between order and disorder, only the existence of overlapping corona layers as a function of concentration. Additional TR-SANS experiments, conducted at intermediate concentrations, below and above the point of ordering, would be necessary to determine whether the kinetic slow down is linked to the state of long-range order. Furthermore, this hypothesis suggests that as the melt state is approached, where the corona crowding effect vanishes due to the screening of excluded volume, the barrier to expulsion

might actually go down again, which suggests a promising future avenue for experiments.

SUMMARY

Single chain exchange in bcc-ordered mixtures of PS−PEP diblock copolymer (15% by volume) and squalane has been measured as a function of temperature for two molecular weight specimens. Mixtures of selectively deuterated (dPS−PEP) and protonated (hPS−PEP) polymer in contrast matched squalane ($C_{30}H_{62}/C_{30}D_{32}$) were mechanically blended at room temperature, well below the glass transition temperature of the PS micelle cores. TR-SANS experiments, performed between 110 and 165 °C, evidence molecular exchange as a function of time through changes in the SANS intensity associated with the mixing of dPS and hPS blocks. After accounting for the effects of temperature, these results reveal a dramatic slowing down in the exchange dynamics relative to previous findings with disordered 1% PS−PEP micellar mixtures, although both conform to an approximately logarithmic relaxation function. These results are tentatively attributed to the high concentration of the corona chains, which presents a further barrier to the expulsion of individual core blocks from the micelle cores. However, other explanations cannot yet be excluded, so further study is warranted.

ASSOCIATED CONTENT

Supporting Information. Additional SAXS data including concentration dependence of the relaxation function in dilute solutions and sensitivity of calculated $R(t)$ to variation in the interfacial tension. This material is available free of charge via the Internet at http://pubs.acs.org.

AUTHOR INFORMATION

Corresponding Author

*E-mail: (F.S.B.) bates@cems.umn.edu; (T.P.L.) lodge@umn.edu.

ACKNOWLEDGMENT

This work was supported by Infineum USA L.P. and by the MRSEC program of the National Science Foundation under Grant No. DMR-0819885. We acknowledge the support of the National Institute of Standards and Technology (NIST), U.S. Department of Commerce, in providing the neutron research facilities used in this work. We thank Dr. Paul Butler and Dr. Yun Liu at NIST for assistance with SANS measurements.

REFERENCES

(1) Hamley, I. W., *The Physics of Block Copolymer*: Oxford University: New York, 1998.
(2) Tian, M.; Qin, A.; Ramireddy, C.; Webber, S. E.; Munk, P.; Tuzar, Z.; Procházka, K. *Langmuir* **1993**, *9*, 1741–1748.
(3) Honda, C.; Hasegawa, Y.; Hirunuma, R.; Nose, T. *Macromolecules* **1994**, *27*, 7660–7668.
(4) Honda, C.; Abe, Y.; Nose, T. *Macromolecules* **1996**, *29*, 6778–6785.
(5) Goldmints, I.; Holzwarth, J. G.; Smith, K. A.; Hatton, T. A. *Langmuir* **1997**, *13*, 6130–6134.
(6) Waton, G.; Michels, B.; Zana, R. *Macromolecules* **2001**, *34*, 907–910.
(7) Procházka, K.; Bednář, B.; Mukhtar, E.; Svoboda, P.; Trněná, J.; Almgren, M. *J. Phys. Chem.* **1991**, *95*, 4563–4568.
(8) Procházka, K.; Kiserow, D.; Ramireddy, C.; Tuzar, Z.; Munk, P.; Webber, S. E. *Macromolecules* **1992**, *25*, 454–460.
(9) Wang, Y.; Kausch, C. M.; Chun, M.; Quirk, R. P.; Mattice, W. L. *Macromolecules* **1995**, *28*, 904–911.
(10) Smith, C. K.; Liu, G. *Macromolecules* **1996**, *29*, 2060–2067.
(11) Underhill, R. S.; Ding, J.; Briss, V. I.; Liu, G. *Macromolecules* **1997**, *30*, 8298–8303.
(12) Zhang, L.; Shen, H.; Eisenberg, A. *Macromolecules* **1997**, *30*, 1001–1011.
(13) Esselink, F.; Dormidontova, E.; Hadziioannou, G. *Macromolecules* **1998**, *31*, 2925–2932.
(14) Esselink, F.; Dormidontova, E.; Hadziioannou, G. *Macromolecules* **1998**, *31*, 4873–4878.
(15) Won, Y.; Davis, H. T.; Bates, F. S. *Macromolecules* **2003**, *36*, 953–955.
(16) Willner, L.; Poppe, A.; Allgaier, J.; Monkenbusch, M.; Richter, D. *Europhys. Lett.* **2001**, *55*, 667–673.
(17) Lund, R.; Willner, L.; Stellbrink, J.; Lindner, P.; Richter, D. *Phys. Rev. Lett.* **2006**, *96*, 068302.
(18) Lund, R.; Willner, L.; Richter, D.; Dormidontova, E. E. *Macromolecules* **2006**, *39*, 4566–4575.
(19) Lund, R.; Willner, L.; Richter, D.; Iatrou, H.; Hadjichristidis, N.; Lindner, P. *J. Appl. Crystallogr.* **2007**, *40*, s327–s331.
(20) Choi, S.; Lodge, T. P.; Bates, F. S. *Phys. Rev. Lett.* **2010**, *104*, 047802.
(21) Halperin, A.; Alexander, S. *Macromolecules* **1989**, *22*, 2403–2412.
(22) Dormidontova, E. E. *Macromolecules* **1999**, *32*, 7630–7644.
(23) Anderson, J. A.; Lorenz, C. D.; Travesset, A. *J. Chem. Phys.* **2008**, *128*, 184906.
(24) McConnell, G. A.; Gast, A. P.; Huang, J. S.; Smith, S. D. *Phys. Rev. Lett.* **1993**, *71*, 2102–2105.
(25) Watzlawek, M.; Likos, C. N.; Löwen, H. *Phys. Rev. Lett.* **1999**, *82*, 5289–5292.
(26) Hanley, K. J.; Lodge, T. P.; Huang, C.-I. *Macromolecules* **2000**, *33*, 5918–5931.
(27) Lodge, T. P.; Bang, J.; Park, M. J.; Char, K. *Phys. Rev. Lett.* **2004**, *92*, 145501.
(28) Grason, G. M. *J. Chem. Phys.* **2007**, *126*, 114904.
(29) Choi, S.; Lodge, T. P.; Bates, F. S. *J. Phys. Chem. B* **2009**, *113*, 13840–13848.
(30) Hahn, S. F. *J. Polym. Sci., Polym. Chem.* **1992**, *30*, 397–408.
(31) Nicholson, J. C.; Crist, B. *Macromolecules* **1989**, *22*, 1704–1708.
(32) Choi, S.; Lee, S.; Soto, H. E.; Lodge, T. P.; Bates, F. S. *J. Am. Chem. Soc.* **2010**, *133*, 1722–1725.
(33) Glinka, C. J.; Barker, J. G.; Hammouda, B.; Krueger, S.; Moyer, J. J.; Orts, W. J. *J. Appl. Crystallogr.* **1998**, *31*, 430–445.
(34) Kline, S. R. *J. Appl. Crystallogr.* **2006**, *39*, 895–900.
(35) Higgins, J. S. Benoît, H. C. *Polymers and Neutron Scattering*; Oxford University: New York, 1994.
(36) Benoît, H.; Koberstein, J.; Leibler, L. *Makromol. Chem. Suppl.* **1981**, *4*, 85–99.
(37) Bates, F. S.; Berney, C. V.; Cohen, R. E.; Wignall, G. D. *Polymer* **1983**, *24*, 519–524.
(38) Matsushita, Y.; Nakao, Y.; Saguchi, R.; Mori, K.; Choshi, H.; Muroga, Y.; Noda, I.; Nagasawa, M.; Chang, T.; Glinka, C. J.; Han, C. C. *Macromolecules* **1988**, *21*, 1802–1806.
(39) Matsushita, Y.; Mori, K.; Mogi, Y.; Saguchi, R.; Noda, I.; Nagasawa, M.; Chang, T.; Glinka, C. J.; Han, C. C. *Macromolecules* **1990**, *23*, 4317–4321.
(40) Willner, L.; Lund, R.; Monkenbusch, M.; Holderer, O.; Colmenero, J.; Richter, D. *Soft Matter* **2010**, *6*, 1559–1570.
(41) Akcasu, A. Z.; Summerfield, G. C.; Jahshan, S. N.; Han, C. C.; Kim, C. Y.; Yu, H. *J. Polym. Sci., Polym. Phys. Ed.* **1980**, *18*, 863–869.
(42) Wignall, G. D.; Hendricks, R. W.; Koehler, W. C.; Lin, J. S.; Wai, M. P.; Thomas, E. L.; Stein, R. S. *Polymer* **1981**, *22*, 886–889.

(43) Wignall, G. D.; Melnichenko, Y. B. *Rep. Prog. Phys.* **2005**, *68*, 1761–1810.
(44) Willner, L.; Jucknischke, O.; Richter, D.; Roovers, J.; Zhou, L.-L.; Toporowski, P. M.; Fetters, L. J.; Huang, J. S.; Lin, M. Y.; Hadjichristidis, N. *Macromolecules* **1994**, *27*, 3821–3829.
(45) Benmouna, M.; Hammouda, B. *Prog. Polym. Sci.* **1997**, *22*, 49–92.
(46) Haliloğlu, T.; Bahar, I.; Erman, B.; Mattice, W. *Macromolecules* **1996**, *29*, 4761–4771.
(47) Mutual-diffusion coefficient of polystyrene in toluene (less than 30 wt % of PS) was reported to be an order of $10^{-7}-10^{-11}$ cm^2 s^{-1}, and self-diffusion coefficient of PS in PS matrix was reported to be an order of 10^{-17} cm^2 s^{-1}:Kim, H.; Chang, T.; Yohanan, J. M.; Wang, L.; Yu, H. *Macromolecules* **1986**, *19*, 2737−2744, and Eastman, C. E.; Lodge, T. P. *Macromolecules* **1994**, *27*, 5591–5598.
(48) Barrat, J.-L.; Fredrickson, G. H. *Macromolecules* **1991**, *24*, 6378–6383.
(49) Dalvi, M. C.; Lodge, T. P. *Macromolecules* **1993**, *26*, 859–861.
(50) Yokoyama, H.; Kramer, E. J. *Macromolecules* **1998**, *31*, 7871–7876.
(51) Cavicchi, K. A.; Lodge, T. P. *Macromolecules* **2003**, *36*, 7158–7164.
(52) Lund, R.; Willner, L.; Stellbrink, J.; Lindner, P.; Richter, D. *Phys. Rev. Lett.* **2010**, *104*, 049902.
(53) Wu, C.; Wang, X. *Phys. Rev. Lett.* **1998**, *80*, 4092–4094.
(54) Wang, X.; Qiu, X.; Wu, C. *Macromolecules* **1998**, *31*, 2972–2976.
(55) Guinier, A. *X-ray diffraction in Crystals, Imperfect Crystals, and Amorphous Bodies*; Dover: New York, 1994.
(56) Cullity, B. D. Stock, S. R. *Elements of X-ray Diffraction*, 3rd ed.; Prentice Hall: Upper Saddle River, NJ, 2001.
(57) Chapman, B. R.; Hamersky, M. W.; Milhaupt, J. M.; Kostelecky, C.; Lodge, T. P.; von Meerwall, E. D.; Smith, S. D. *Macromolecules* **1998**, *31*, 4562–4573.
(58) Fetters, L. J.; Lohse, D. J.; Richter, D.; Witten, T. A.; Zirkel, A. *Macromolecules* **1994**, *27*, 4639–4647.
(59) Flory, P. J. *J. Chem. Phys.* **1942**, *10*, 51–61.
(60) Huggins, M. L. *J. Am. Chem. Soc.* **1942**, *64*, 1712–1719.
(61) Milner, S. T.; Lacasse, M. -D.; Graessley, W. W. *Macromolecules* **2009**, *42*, 876–886.
(62) Allen, G.; Gee, G.; Mangara, D.; Sims, D.; Wilson, G. J. *Polymer* **1960**, *1*, 467–476.
(63) Since the method of Hildebrand's solubility parameters typically gives a qualitative trend of χ between polymers and solvents, the values are not shown in the context:Lund, R.; Willner, L.; Lindner, P.; Richter, D. *Macromolecules* **2009**, *42*, 2686–2695.
(64) Sakurai, S.; Hashimoto, T.; Fetters, L. J. *Macromolecules* **1995**, *28*, 7947–7949.
(65) Lai, C.; Russel, W. B.; Register, R. A.; Marchand, G. R.; Adamson, D. H. *Macromolecules* **2000**, *33*, 3461–3466.
(66) Maurer, W. W.; Bates, F. S.; Lodge, T. P.; Almdal, K.; Mortensen, K.; Fredrickson, G. H. *J. Chem. Phys.* **1998**, *108*, 2989–3000.
(67) Lodge, T. P. *In Structure and Dynamics of Polymer and Colloidal Systems*; Borsali, R., Pecora, R., Eds.; Kluwer Academic Publishers: Dordrecht, The Netherlands, 2002; Vol. 568, pp 225−262.
(68) Yokoyama, H.; Kramer, E. J.; Fredrickson, G. H. *Macromolecules* **2000**, *33*, 2249–2257.
(69) Yokoyama, H.; Kramer, E. J. *Macromolecules* **2000**, *33*, 954–959.
(70) Yokoyama, H.; Kramer, E. J.; Rafailovich, M. H.; Sokolov, J.; Schwarz, S. A. *Macromolecules* **1998**, *31*, 8826–9930.
(71) Lai, C.; Russel, W. B.; Register, R. A. *Macromolecules* **2002**, *35*, 841–849.